

See discussions, stats, and author profiles for this publication at: <https://www.researchgate.net/publication/263957639>

Catalysts, Kinetics, and Reactive Distillation for Methyl Acetate Synthesis

ARTICLE *in* INDUSTRIAL & ENGINEERING CHEMISTRY RESEARCH · JUNE 2014

Impact Factor: 2.59 · DOI: 10.1021/ie500371c

CITATIONS

3

READS

22

5 AUTHORS, INCLUDING:



Chunshan Li

Chinese Academy of Science, China, Beijing

79 PUBLICATIONS 960 CITATIONS

[SEE PROFILE](#)

Catalysts, Kinetics, and Reactive Distillation for Methyl Acetate Synthesis

Cuncun Zuo,[†] Langsheng Pan,^{*,†} Shasha Cao,[‡] Chunshan Li,[‡] and Suojiang Zhang^{*,‡}

[†]School of Chemical Engineering, Xiangtan University, Yuhu District, Xiangtan 411105, People's Republic of China

[‡]Beijing Key Laboratory of Ionic Liquids Clean Process, State Key Laboratory of Multiphase Complex Systems, Institute of Process Engineering, Chinese Academy of Sciences, Haidian District, Beijing 100190, People's Republic of China

Supporting Information

ABSTRACT: Two novel acidic cation-exchange resins, namely, NKC-9 and D072, were first developed to catalyze the esterification of acetic acid with methanol. Kinetics of methyl acetate synthesis are determined by the experiments in a batch reactor at temperatures from 45 to 60 °C under atmospheric pressure, with molar ratio of reactants ($\theta_{\text{Bo}} = n_{\text{methanol}} : n_{\text{acetic acid}}$) from 0.8 to 1.3. The kinetic data are correlated with the Q-H, E-R, and LHHW and pseudohomogeneous (P-H) models. Then, the reactive distillation process for methyl acetate synthesis is simulated by the Aspen Plus process simulator. Lifetime evaluation of NKC-9 was carried out to study the conversion rate of acetic acid and selectivity of methyl acetate during the long-period running in the fixed-bed reactor. Finally, a series of characterizations such as Fourier transform infrared spectroscopy, X-ray diffraction, and polarizing microscopy were performed to investigate the structure and properties of NKC-9.

1. INTRODUCTION

Methyl acetate is an important organic chemical raw material, and high-purity methyl acetate can be used to synthesize acetic anhydride, methyl acrylate, vinyl acetate, and ethyl amide. Moreover, it plays an important role in the synthesis of coating materials, nitro-cellulose, cellulose acetate, cellulose ethers, and celluloid. Methyl acetate also has wide applications in the various industries, which mainly produce essences, plasticizers, and certain fats.^{1–6}

The distillation column reactor packed with ion-exchange resin offers significant superiorities over the routine method of conducting the sequential reaction and separation sequentially.^{7–9} Kinetics of the esterification of propionic acid with *n*-butanol over Amberlyst 35 was investigated under different experimental conditions.¹⁰ Lee et al.¹¹ investigated the kinetic behaviors of the catalytic esterification of amyl alcohol acetate in a fixed-bed reactor using Dowex 50Wx8-100 (an acidic cation-exchange resin) as the catalyst. Xu et al.¹² successfully obtained glycolic acid by hydrolysis of methyl glycolate over ion-exchange resin. Chang et al.¹³ used the Newton homotopy arc length differential method to simulate the synthesis of ethyl acetate by catalytic reactive distillation. Song et al.¹⁴ studied the effect of heterogeneous catalysis on the transition from the nonreactive stage to the reaction equilibrium, and developed a heterogeneous Langmuir–Hinshelwood–Hougen–Watson (LHHW) type reaction rate model for the synthesis of methyl acetate. The nonrandom two-liquid (NRTL) model was used to correct the nonideality of the liquid phase in the reaction system of *n*-butyl alcohol propionate synthesis.¹⁵

In the present study, two strongly acidic cation-exchange resins (NKC-9 and D072) were developed for the catalytic esterification to synthesize methyl acetate. The kinetics experiments were conducted in a batch reactor under different conditions. Given that there was great deviation of the reaction system from the ideal solution, the NRTL model was chosen to

correct the nonideality of the liquid phase. The kinetic data were correlated with the Q-H, E-R, LHHW, and P-H models. Then, simulation and calculation of the catalytic esterification to synthesize methyl acetate in the catalytic distillation column were carried out.

2. EXPERIMENTAL SECTION

2.1. Materials. Acetic acid and methanol were purchased from Sinopharm Chemical Reagent Co., Ltd., both of which were of analytical grade. Hydrochloric acid and sodium chloride were also obtained from the same chemical reagent factory. Distilled water was used for the preparation of all solutions. D072 and NKC-9 were manufactured by Chemical Plant of Nankai University (China). Before D072 and NKC-9 were used for the catalysts for the esterification reaction, the purchased resins were soaked in the saturated NaCl solution for 8 h to remove certain impurities. To ensure that the pH of two cation-exchange resins was 7, the resins were washed with HCl solution and distilled water sequentially.

2.2. Apparatus and Procedure. The kinetics experiments of the esterification of methyl acetate were performed in a 250 mL three-necked flask equipped with a reflux condensing tube, a sampling device, and a thermometer. The reaction temperature was controlled to within ± 0.1 K by Super thermostat water bath. First, acetic acid and the catalyst were placed the reactor and heated to the desired reaction temperature. Methanol preheated to the reaction temperature was then added into the reactor through a constant pressure drop funnel to start the esterification reaction. The course of the reaction was monitored by determining of the composition of small

Received: January 26, 2014

Revised: June 2, 2014

Accepted: June 12, 2014

Published: June 23, 2014



samples which were withdrawn from the liquid mixture at regular intervals. After a steady state was achieved, the product was collected in a sampling flask.

Product samples were analyzed by gas chromatography (GC6890, made in China) with a flame ionization detector and a chromatographic capillary column PEG-20M ($30\text{ m} \times 0.20\text{ mm} \times 0.25\mu\text{m}$). The column temperature rose to $160\text{ }^{\circ}\text{C}$ by a programmed temperature method. The vaporizing chamber and detector temperatures were set at $180\text{ }^{\circ}\text{C}$. High purity nitrogen gas ($>99.999\%$) was used as carrier. The conversion rate of acetate acid is defined as the ratio between the amount of acetate acid transformed and the total amount of acetate acid.

Pretreated NKC-9 beads with an average particle size of 35 meshes and glass wool were packed in a fixed-bed reactor. The catalyst load (W) was $0.025\text{ g catalyst/g liquid mixture}$ for the base case. With different space-times, the experiment was repeated to investigate the effect of space-time on the conversion rate of acetic acid.

2.3. Characterizations. The surface morphology of NKC-9 was observed by scanning electron microscopy (SEM; Quanta250; EDAX Genesis-SiLi). Pore size diameter distribution curve of the fresh NKC-9 was recorded on a Automatic mercury analyzer (AutoPore IV 9510), which includes two low voltage stations and a high voltage station. Pores ranging in size from 50 \AA to $1000\text{ }\mu\text{m}$ can be measured by this Automatic mercury analyzer.

Elements content of the fresh NKC-9 was determined by an elemental analyzer (Vario EL cube, Germany), which is provided with high measurement accuracy.

The Fourier transform infrared spectroscopy (FT-IR) spectra of the fresh and regenerative NKC-9 were recorded on a NICOLET 380 spectrometer (Thermo Nicolet Corporation, USA) in the optical range of $500\text{--}4000\text{ cm}^{-1}$ by averaging 32 scans at a resolution of 4 cm^{-1} .

XRD patterns of the fresh and regenerative NKC-9 catalyst were obtained using a power X-ray diffractometer (Rigaku Dmax-C) with $\text{Cu K}\alpha$ radiation ($k = 1.5405\text{ \AA}$). The XRD patterns were obtained from $2\theta = 10^{\circ}$ to 90° .

The differences of the fresh and regenerative NKC-9 were assessed visually using a polarizing microscope (Olympus BX51, Olympus, Melville, NY) at $10\times$ to $50\times$ magnifications.

3. RESULTS AND DISCUSSION

3.1. Selection of Strongly Acidic Cation-Exchange Resin Catalysts. To investigate the catalytic activity of the strongly acidic cation-exchange resins (D072 and NKC-9), a preliminary comparison was performed. As is clearly shown in Figure 1, before reaching the reaction equilibrium, the conversion rate of acetic acid in the presence of NKC-9 was higher than that in the presence of D072. In addition, the required time to reach the reaction equilibrium was relatively shorter with NKC-9 as the catalyst. Moreover, no dimethyl ether was detected in the experiments with NKC-9 as the catalyst, which indicated the high selectivity of NKC-9. However, a small quantity of dimethyl ether was found when D072 was used. Therefore, NKC-9 was selected for further study of the catalytic esterification.

3.2. Kinetics Experiments and Optimization of Esterification Conditions. **3.2.1. Effect of Catalyst Load.** The same experiment was repeated at $45\text{ }^{\circ}\text{C}$ with a molar ratio of reactants of 0.8:1. The effect of catalyst load on the conversion rate of acetic acid was determined by changing the

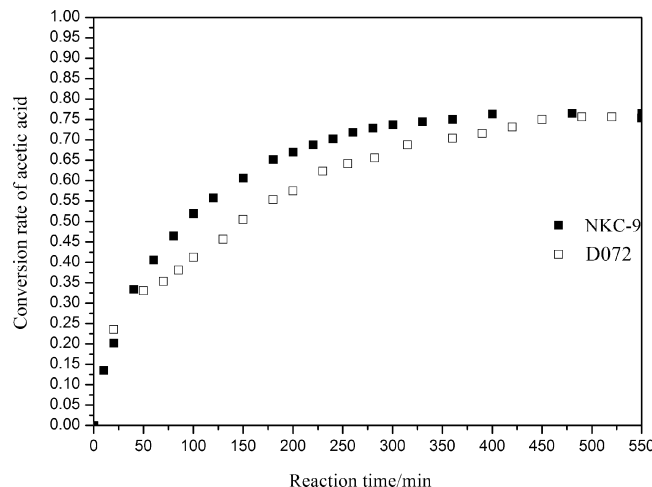


Figure 1. Evaluation of catalytic activity of NKC-9 and D072.

amount of catalyst load. The catalyst load ranged from $0.020\text{ g catalyst/g liquid mixture}$ to $0.030\text{ g/g liquid mixture}$, and blank experiment was also used. As shown in Figure 2, the required

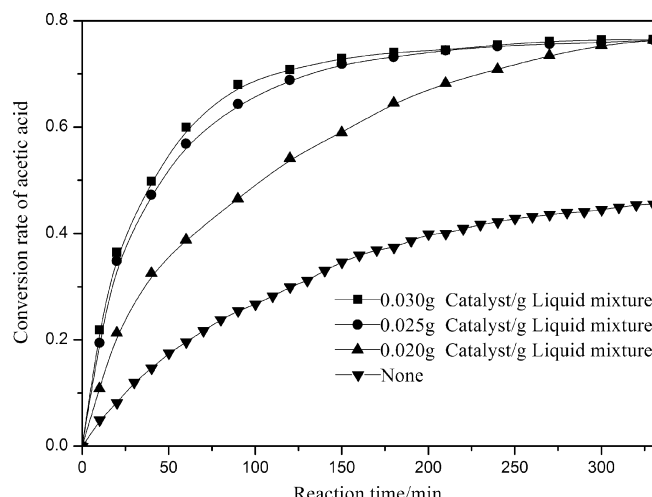


Figure 2. Effect of catalyst load (NKC-9) on the conversion rate of acetic acid ($45\text{ }^{\circ}\text{C}$, $\theta_{\text{Bo}} = 0.8:1$).

time to reach the reaction equilibrium was shortened significantly with the presence of catalyst compared with that of the blank experiment. When the catalyst load was increased from $0.020\text{ g catalyst/g liquid mixture}$ to $0.025\text{ g catalyst/g liquid mixture}$, the conversion rate of acetic acid measured significantly increased under the same reaction time, which was attributed to the increase in available active sites caused by the change in catalyst load. However, when the catalyst load was increased from $0.025\text{ g catalyst/g liquid mixture}$ to $0.030\text{ g catalyst/g liquid mixture}$, the conversion rate of acetic acid measured was nearly identical under the same reaction time. These results demonstrated that $0.025\text{ g catalyst/g liquid mixture}$ was the optimum catalyst load.

3.2.2. Effect of Reaction Temperature. To determine the effect of reaction temperature on the catalytic esterification, the same experiment was repeated at different reaction temperatures, i.e., 45 , 50 , 55 , and $60\text{ }^{\circ}\text{C}$, with a catalyst load of $0.025\text{ g catalyst/g liquid mixture}$ and a molar ratio of reactants of $0.8:1$. As shown in Figure 3, before the reaction equilibrium was

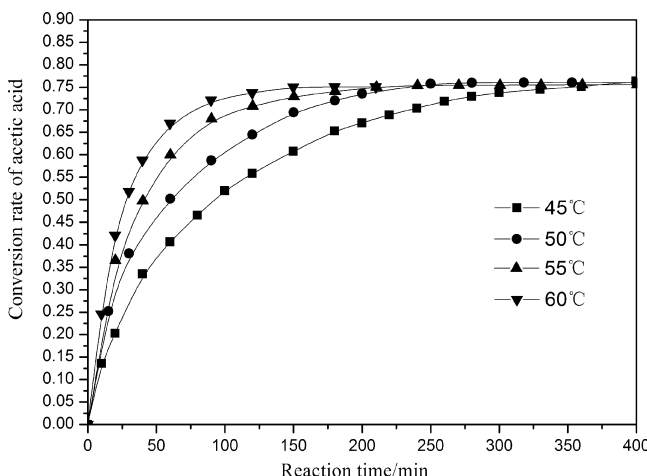


Figure 3. Effect of reaction temperature on the conversion rate of acetic acid using NKC-9 as the catalyst ($\theta_{B_0} = 0.8:1$, and the catalyst load was 0.025 g catalyst/g liquid mixture).

reached, the conversion rate of acetic acid significantly increased with temperature under the same reaction time, which indicated that high temperature facilitates the forward reaction. This result is attributed to the partial vaporization of the aqueous mixtures at high temperatures and long contact times. However, the disparity among the equilibrium conversion rate of acetic acid is very small in the temperature range studied. Sanz et al.¹⁶ have also obtained similar results in methyl lactate hydrolysis.

3.2.3. Effect of Molar Ratio of Reactants. To determine the optimum molar ratio of reactants (θ_{B_0}), the same experiment was repeated with different reactant molar ratios (θ_{B_0}) containing 0.8:1, 1.0:1, 1.1:1, 1.2:1, and 1.3:1 at 60 °C, and the catalyst load was 0.025 g catalyst/g liquid mixture. According to the theories of chemical equilibrium, increasing the reactant ratio can enhance the conversion rate of methyl acetate. However, acetic acid has a high boiling point, and it is provided at a smaller proportion in the vapor phase. Hence, the yield of methyl acetate is calculated on the basis of the conversion rate of acetic acid. In the present study, when the molar ratio of reactants was increased from 0.8:1 to 1.3:1 in the primary stage of the reaction, a significant increase in the conversion rate of acetic acid was found (Figure 4). When the molar ratio of reactants was increased from 0.8:1 to 1.2:1, the equilibrium conversion rate of acetic acid increased as well. Nevertheless, when the reactant molar ratio was increased from 1.2:1 to 1.3:1, the equilibrium conversion rate of acetic acid changed insignificantly. This phenomenon was attributed to the difficulties in the separation of methyl acetate at higher molar ratio of reactants when the reaction is close to equilibrium.

3.2.4. Elimination of External Diffusion. To study the reaction kinetics of the system, the effect of external diffusion must be excluded. External diffusion effects could be eliminated by increasing the stirring speed at the optimum catalyst load, reaction time, and molar ratio of reactants aforementioned. To determine a suitable stirring speed, the same experiment was repeated under different stirring speeds including 400, 500, and 600 rpm. The experimental results are shown in Figure 5. When the stirring speed was increased from 350 to 450 rpm, a significant increase in the conversion rate of acetic acid was found at the same reaction time. However, when the stirring speed was increased from 450 to 550 rpm, the conversion rate

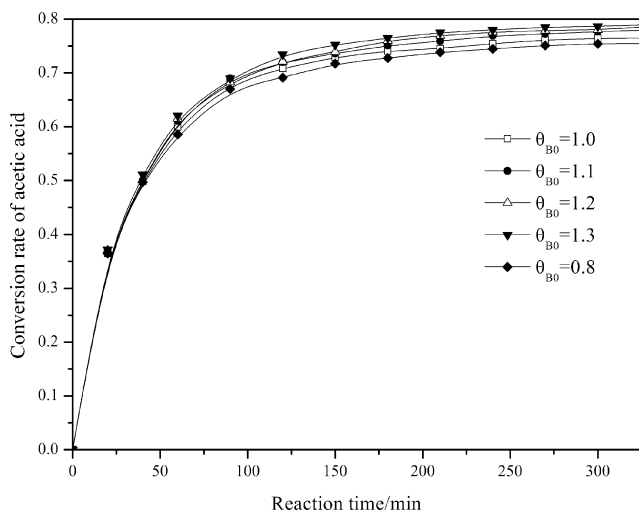


Figure 4. Effect of molar ratio of reactants on the conversion rate of acetic acid using NKC-9 as catalyst (60 °C, and the catalyst load was 0.025 g catalyst/g liquid mixture).

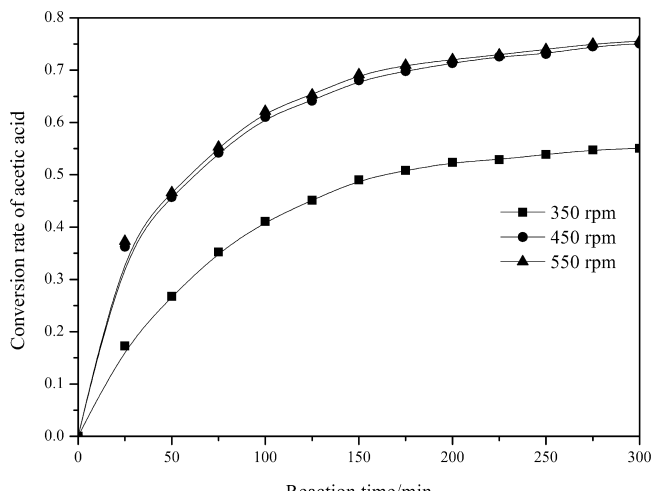


Figure 5. Effect of stirring speed on the conversion rate of acetic acid using NKC-9 as catalyst (60 °C; $\theta_{B_0} = 1.2:1$; the catalyst load was 0.025 g catalyst/g liquid mixture).

of acetic acid was almost constant. Therefore, the effect of external diffusion can be eliminated when the stirring speed is >450 rpm. Given the serious abrasion on equipment and large energy consumption caused by high stirring speed, 450 rpm was used.

3.2.5. Elimination of Internal Diffusion. To investigate the effect of internal diffusion on catalytic esterification, commercial NKC-9 was screened into several different particle sizes, including 24, 28, 32, and 35 meshes. The same experiment was repeated with different catalyst particle sizes at the optimal catalyst load, reaction time, and molar ratio of reactants aforementioned. As shown in Figure 6, when the catalyst particle size is >28 meshes, the conversion rate of acetic acid was unaffected by the catalyst particle size. However, when the catalyst particle size is <28 meshes, the conversion rate of acetic acid was significantly decreased. The results are consistent with the theoretical calculations reported by Xu et al.¹⁷ Internal diffusion was only found in the catalyst with a particle size <28 meshes. In addition, given the decrease in the size of catalyst, more active sites are exposed, which facilitated the reaction.

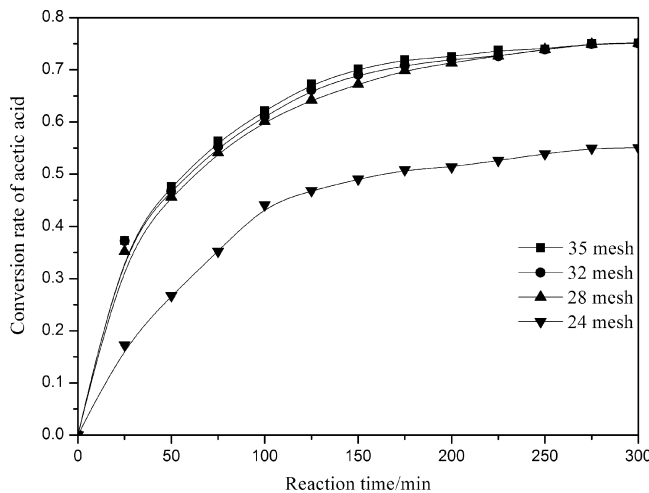


Figure 6. Effect of catalyst particle size on the conversion rate of acetic acid using NKC-9 as catalyst (60°C ; $\theta_{\text{Bo}} = 1.2:1$; the catalyst load was 0.025 g catalyst/g liquid mixture).

3.3. Kinetic Model and Equilibrium Constant. The esterification reaction can be expressed by the following equation:



where A , B , C , and D refer to acetic acid, methanol, methyl acetate and water, respectively.

The equilibrium concentration ratio (K_x) of the esterification is obtained from equilibrium conversion rate (X_{Ac}) and molar ratio of reactants (θ_{Bo}):

$$K_x = \frac{X_{\text{Ac}}^2}{(1 - X_{\text{Ac}})(\theta_{\text{Bo}} - X_c)} \quad (2)$$

The introduction of activities in kinetics study contributes to a smaller error.^{18–21} And the equilibrium constant in terms of activity is defined as

$$K_{\text{eq}} = \frac{a_3 \cdot a_4}{a_1 \cdot a_2} = \frac{x_3 \cdot \gamma_3 \times x_4 \cdot \gamma_4}{x_1 \cdot \gamma_1 \times x_2 \cdot \gamma_2} = \frac{x_3 \cdot x_4}{x_1 \cdot x_2} \times \frac{\gamma_3 \cdot \gamma_4}{\gamma_1 \cdot \gamma_2} = K_x \times K_{\gamma} \quad (3)$$

$\ln K_{\text{eq}}$ varies linearly with $1/T$ at temperatures $<60^{\circ}\text{C}$. The relationship is given by

$$\ln K_{\text{eq}} = 2565.1/T - 4.7335 \quad (4)$$

$$\Delta G^o = -RT \ln K_{\text{eq}} = -21.3262 \times 10^3 + 39.3543T \quad (5)$$

The calculated values of K_{γ} and K_{eq} are clearly shown in Table 1.

The kinetic data were correlated with a mass-balance equation for acetic acid listed as follows:

$$W/(10^3 F_A) = \int_0^{X_A} \frac{dX_A}{-r_A} \quad (6)$$

Table 1. Values of K_{γ} and K_{eq}

temperature (K)	K_{γ}	K_{eq}
318.15	4.9072	28.2495
323.15	4.3777	24.0505
328.15	4.2103	22.1038
333.15	3.8656	19.4203

where W is the catalyst load; F_A is the volumetric flow rates of acetic acid; X_A is the conversion rate of acetic acid; $-r_A$ is the rate expression. The right-hand side integral in eq 6 was determined using the Simpson formula. The optimum values of the kinetic parameters were obtained by minimizing the following objective function (π) with a modified Levenberg–Marquardt algorithm:⁴

$$\pi = \sum_{i=1}^N \left[\left(\frac{1}{RHS} \right)_i - \left(\frac{10^3 F_A}{W} \right)_i \right]^2 \quad (7)$$

The rate expression $-r_A$ is determined by the hypothesis of the reaction mechanism. The Q-H, E-R, and LHHW models of Gonzalez and Fair²² were adopted to investigate the kinetics of the catalytic esterification process. Given the relatively stronger water affinity of resins, the adsorption of methanol, acetic acid, and methyl acetate were omitted in the Q-H and E-R models. The rate expressions of the Q-H^{IS}, Q-H^{NIS}, and E-R and models are listed as follows:

(a) the Q-H^{IS} model (ideal-solution assumption)

$$-r_A = A_+ \exp\left(\frac{-E_+}{RT}\right) \left[x_A x_B - \frac{A_-}{A_+} \exp\left(\frac{\Delta H}{RT}\right) x_C x_D \right] \quad (8)$$

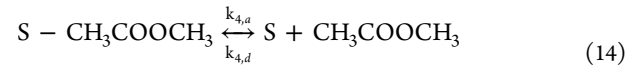
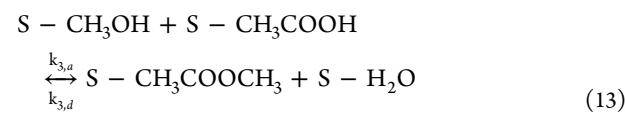
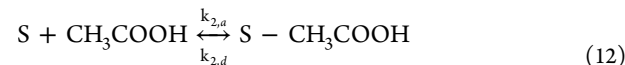
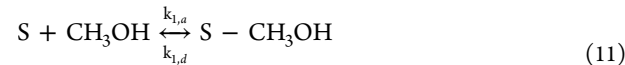
(b) the Q-H^{NIS} model (non-ideal-solution assumption)

$$-r_A = A_+ \exp\left(\frac{-E_+}{RT}\right) \left[a_A a_B - \frac{A_-}{A_+} \exp\left(\frac{\Delta H}{RT}\right) a_C a_D \right] \quad (9)$$

(c) the E-R model

$$-r_A = \frac{A_+ \exp\left(\frac{-E_+}{RT}\right) \left[a_A a_B - \frac{A_-}{A_+} \exp\left(\frac{\Delta H}{RT}\right) a_C a_D \right]}{(1 + K_D a_D)} \quad (10)$$

The derivation process of the LHHW model is described as follows:



The surface reaction is usually the rate-controlling step in the catalytic esterification over strongly acidic cation-exchange resin catalyst, i.e., Step 13:

$$-r_A = k_{3,a} \theta_{\text{Me}} \theta_{\text{Ac}} - k_{3,d} \theta_{\text{MeAc}} \theta_{\text{H}_2\text{O}} \quad (16)$$

The normalized results were used in the above equations:

$$\theta_{\text{Me}} = \frac{K_1 \alpha_{\text{Me}}}{(1 + K_1 \alpha_{\text{Me}} + K_2 \alpha_{\text{Ac}} + K_4 \alpha_{\text{MeAc}} + K_5 \alpha_{\text{H}_2\text{O}})} \quad (17)$$

$$\theta_{\text{Ac}} = \frac{K_2 \alpha_{\text{Ac}}}{(1 + K_1 \alpha_{\text{Me}} + K_2 \alpha_{\text{Ac}} + K_4 \alpha_{\text{MeAc}} + K_5 \alpha_{\text{H}_2\text{O}})} \quad (18)$$

$$\theta_{\text{MeAc}} = \frac{K_4 \alpha_{\text{MeAc}}}{(1 + K_1 \alpha_{\text{Me}} + K_2 \alpha_{\text{Ac}} + K_4 \alpha_{\text{MeAc}} + K_5 \alpha_{\text{H}_2\text{O}})} \quad (19)$$

$$\theta_{\text{H}_2\text{O}} = \frac{K_5 \alpha_{\text{H}_2\text{O}}}{(1 + K_1 \alpha_{\text{Me}} + K_2 \alpha_{\text{Ac}} + K_4 \alpha_{\text{MeAc}} + K_5 \alpha_{\text{H}_2\text{O}})} \quad (20)$$

$$\begin{aligned} -r_A &= k_{3,a} \theta_{\text{Me}} \theta_{\text{Ac}} - k_{3,d} \theta_{\text{MeAc}} \theta_{\text{H}_2\text{O}} \\ &= \frac{k_{3,a} K_1 K_2 \alpha_{\text{Me}} \alpha_{\text{Ac}} - k_{3,d} K_4 K_5 \alpha_{\text{MeAc}} \alpha_{\text{H}_2\text{O}}}{(1 + K_1 \alpha_{\text{Me}} + K_2 \alpha_{\text{Ac}} + K_4 \alpha_{\text{MeAc}} + K_5 \alpha_{\text{H}_2\text{O}})^2} \end{aligned} \quad (21)$$

$$\begin{aligned} -r_A &= \frac{k_{3,a} K_1 K_2 \left(\alpha_{\text{Me}} \alpha_{\text{Ac}} - \frac{k_{3,d} K_4 K_5}{k_{3,a} K_1 K_2} \alpha_{\text{MeAc}} \alpha_{\text{H}_2\text{O}} \right)}{(1 + K_1 \alpha_{\text{Me}} + K_2 \alpha_{\text{Ac}} + K_4 \alpha_{\text{MeAc}} + K_5 \alpha_{\text{H}_2\text{O}})^2} \\ &= \frac{k_+ (\alpha_{\text{Me}} \alpha_{\text{Ac}} - \alpha_{\text{MeAc}} \alpha_{\text{H}_2\text{O}} / K_{\text{eq}})}{(1 + K_1 \alpha_{\text{Me}} + K_2 \alpha_{\text{Ac}} + K_4 \alpha_{\text{MeAc}} + K_5 \alpha_{\text{H}_2\text{O}})^2} \end{aligned} \quad (22)$$

According to the method mentioned in the previous studies,^{14,22} the adsorption equilibrium constants and corresponding equation were obtained after performing adsorption experiments:

$$K_1 = 4.95; \quad K_2 = 3.18; \quad K_4 = 4.16; \quad K_5 = 5.24$$

$$k_+ = A_+ \exp\left(\frac{-E_+}{RT}\right) = 5.1093 \times 10^{10} \exp(-52275.94/RT) \quad (23)$$

The values of K_1 , K_2 , K_3 , K_4 , k_+ , and K_{eq} were substituted into the rate expression (eq 22), and the rate expression of the esterification reaction was obtained:

$$-r_A = \frac{5.1093 \times 10^{10} \exp\left(-\frac{52275.94}{RT}\right) [\alpha_{\text{Me}} \alpha_{\text{Ac}} - \alpha_{\text{MeAc}} \alpha_{\text{H}_2\text{O}} / \exp(2565.1/T - 4.7335)]}{(1 + 4.95 \alpha_{\text{Me}} + 3.18 \alpha_{\text{Ac}} + 4.16 \alpha_{\text{MeAc}} + 5.24 \alpha_{\text{H}_2\text{O}})^2} \quad (24)$$

The data correlation results of the Q-H^{IS}, Q-H^{NIS}, E-R, and LHHW models are listed in Table 2.

Table 2. Results of the Data Correlation of the Q-H^{IS}, Q-H^{NIS}, E-R, and LHHW Models

model	Q-H ^{IS}	Q-H ^{NIS}	E-R	LHHW
$10^{-10} A_+$ (mol min ⁻¹ kg ⁻¹)	3.7919	4.0720	6.8958	5.1093
E_+ (kJ mol ⁻¹)	36.5	44.7	46.8	52.3
A_+/A_-	0.1913	0.2589	0.2102	0.2798
$\Delta H/R$	901.223	934.584	947.254	962.074
K_D			8.5246	
π^a (mol ² min ⁻² kg ⁻²)	4.2136	3.7891	1.7542	1.2503
AAD^b (mol min ⁻¹ kg ⁻¹)	0.1748	0.1425	0.1425	0.1067
bias. ^c (mol min ⁻¹ kg ⁻¹)	0.08580	0.04215	-0.00354	0.00524

^aDefined in eq 7. ^bAAD = N $\sum_{i=1}^N |(1/RHS)_i - (10^3 F_A/W_i)|$. ^cBias = 1/N $\sum_{i=1}^N |(1/RHS)_i - (10^3 F_A/W_i)|$.

The Q-H^{IS} model correlated the kinetic data to a sum of square deviations (π) of 4.2 mol² min⁻² kg⁻². When the nonideality of the reaction system was considered in the Q-H^{NIS} model, the value of π was 3.8 mol² min⁻² kg⁻². Results demonstrated that the E-R model is better than the Q-H^{IS} and Q-H^{NIS} models. However, the E-R model did not improve the correlation. Results indicated that the LHHW model was capable of representing the kinetic behavior of the liquid–solid catalytic esterification under the current experimental conditions.

A pseudohomogeneous model (P-H) was also investigated. The P-H model is derived from the regression of experimental data. Compared with the LHHW model, the P-H model neglects adsorption effects between the ion-exchange resin catalysts and components caused by molecular size and polarity. However, the results fitted well when the P-H model was incorporated into the simulation. The equations of

equilibrium constant, rate constant, and reaction rate were listed as follows:

$$k_{+1} = 14192.5 \exp\left(\frac{-52275.94}{RT}\right) \text{ mol gL}^{-1} \text{ gS}^{-1} \quad (25)$$

$$k_{-1} = 50723.73 \exp\left(\frac{-60274.62}{RT}\right) \text{ mol gL}^{-1} \text{ gS}^{-1} \quad (26)$$

$$K_c = 0.2798 \exp\left(\frac{7998.68}{RT}\right) \quad (27)$$

$$-r_A = k_{+1} (C_{\text{MeOAc}} C_{\text{H}_2\text{O}} - C_{\text{HOAc}} C_{\text{MeOH}} / K_c) \quad (28)$$

Considering that the reaction system of methyl acetate synthesis greatly deviated from ideal solution, the NRTL model was chosen to correct the nonideality of the liquid phase. In this paper, binary interaction parameters are regressed by VLE data, and the activity coefficients are calculated by NRTL equations. The VLE data originated from the DECHEMA Vapor Liquid Equilibrium Data Collection.^{23–26} Aspen Plus was selected for calculating the NRTL parameters. Considering the association of acetic acid molecules in the vapor phase, the NRTL-HOC thermodynamic model was selected for the simulation. Binary interaction parameters of the NRTL model used for the calculation of activity coefficients are clearly shown in Table 3.

3.4. Determination of Space-Time of the Fixed-Bed Reactor.

The space-time (τ) of the fixed-bed reactor is defined as

$$\tau = V_e/F \quad (29)$$

where V_e is the effective volume of the fixed-bed reactor and F is the volumetric flow rates of the reactants. With different space-time, the experiment was repeated in a fixed-bed reactor packed with NKC-9 to investigate the effect of space-time on the conversion rate of acetic acid under the optimum reaction

Table 3. Binary Interaction Parameters of the NRTL Model for Acetic Acid (1), Methanol (2), Water (3), and Methyl Acetate (4)

$$\ln \gamma_i = \frac{\sum_{j=1}^c \tau_{ji} G_{ji} x_j}{\sum_{k=1}^c G_{ki} x_k} + \sum_{j=1}^c \frac{x_j G_{ij}}{\sum_{k=1}^c G_{ki} x_k} \left[\tau_{ij} - \left(\sum_{r=1}^c x_r \tau_{ri} G_{rj} / \sum_{k=1}^c G_{ki} x_k \right) \right]$$

$$G_{ij} = \exp(-\alpha_{ij} \tau_{ij}) \quad G_{ji} = \exp(-\alpha_{ij} \tau_{ji})$$

$$\tau_{ij} = A_{ij}/T \quad \tau_{ji} = A_{ji}/T \quad \tau_{ii} = \tau_{jj} = 0$$

(i,j)	A _{ij} (K)	A _{ji} (K)	α _{ij}
(1,2)	342.0151	-310.2822	0.30
(1,3)	-48.5157	385.2682	0.30
(1,4)	-239.2462	415.2702	0.30
(2,3)	-57.8859	292.9637	0.30
(2,4)	130.5047	234.8660	0.30
(3,4)	866.2183	269.5857	0.35

conditions obtained from the experiments in the batch reactor. As shown in Figure 7, when the space-time was increased to

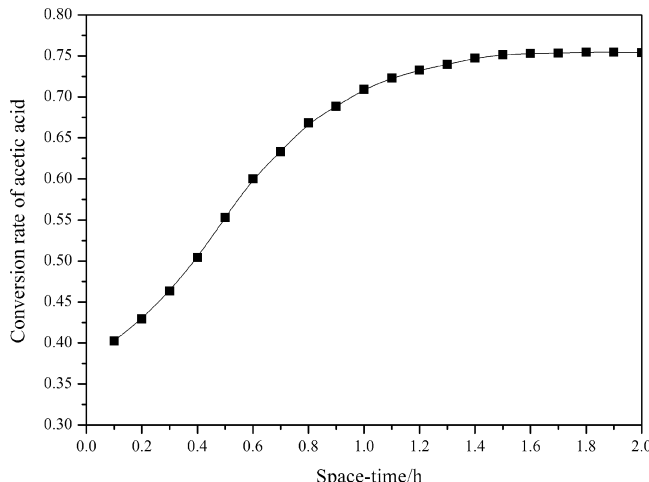


Figure 7. Effect of space-time for the fixed-bed reactor on the conversion rate of acetic acid (60 °C; θ_{Bo} = 1.2:1; 450r/min; the catalyst particle size and catalyst load were 40 meshes and 0.025 g catalyst/g liquid mixture, respectively).

from 0.1 to 1.5 h, a significant increase in the conversion rate of acetic acid was found. However, when the space-time was increased from 1.5 to 2.0 h, the conversion rate of acetic acid was almost constant. These results demonstrated that 1.5 h was the most appropriate space-time for the fixed-bed reactor.

3.5. Reaction Distillation. A catalytic distillation column was used for the process simulation of methyl acetate synthesis, which comprised mainly a rectifying section, extractive distillation section, reaction section, and stripping section. As is clearly shown in Figure 8, acetic acid was introduced into the higher section of the column (rectifying section). Meanwhile, methanol was introduced into the stripping section of the column. The two reactants reacted at the reactive section of the catalytic distillation column, which was packed with pretreated NKC-9. Methyl acetate, which was obtained from the esterification of acetic acid with methanol over NKC-9 catalyst, formed an azeotrope with methanol. When the azeotrope passed through the extractive distillation section, the azeotrope system was broken by acetic acid, and then high purity methyl acetate was collected at the top of the catalytic distillation

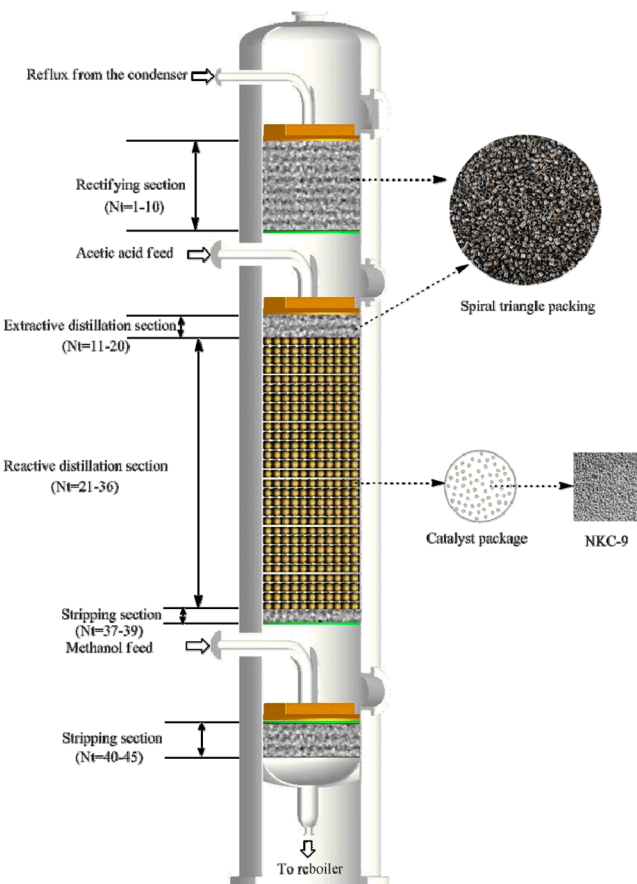


Figure 8. Schematic diagram of catalytic distillation column.

column. The azeotropic temperatures and compositions are listed in Table 4.

Table 4. Azeotropic Temperatures and Compositions (Molar Fraction)

system	T (K)	x _{methyl acetate}	x _{methanol}	x _{H₂O}
methyl acetate–methanol	329.469	0.9155	0	0.0845
methyl acetate–H ₂ O	326.437	0.6669	0.3331	0

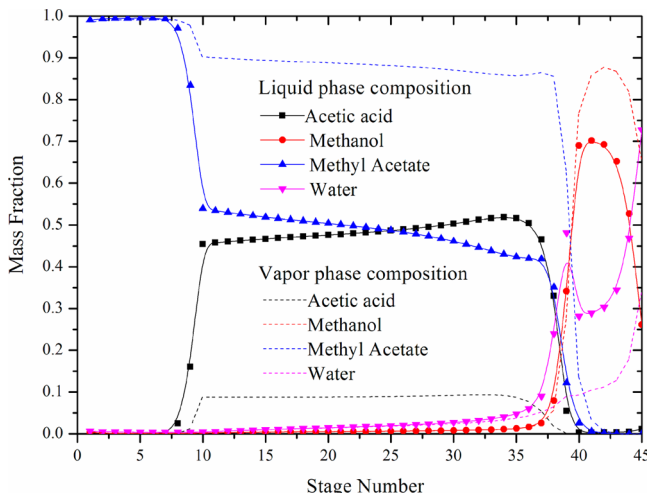
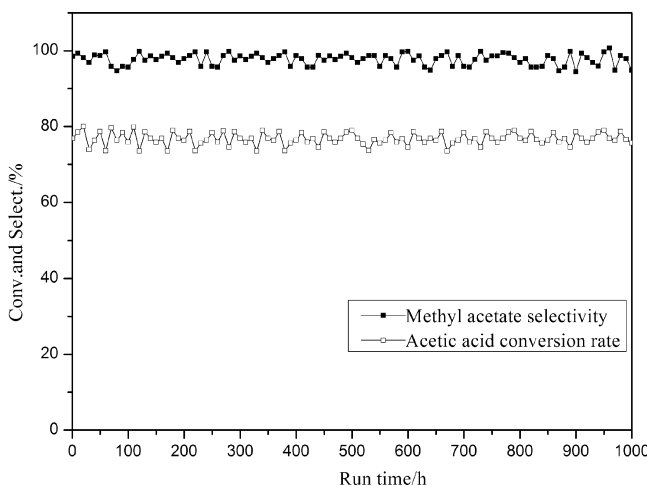
The equilibrium stage model was used to the process simulation of methyl acetate synthesis in the catalytic distillation column. The Newton homotopy arc length differential method with a good convergence was chosen to solve the simultaneous nonlinear equations. And the satisfactory results were obtained. The parameters and results of simulation and optimization are shown in Table 5, and the vapor–liquid composition distribution in the catalytic distillation column is illustrated by Figure 9.

3.6. Long Life of NKC-9. As shown in Figure 10, after a long period of running in the fixed-bed reactor, the catalyst still shows the high conversion rate of acetic acid and selectivity of methyl acetate, which convincingly verified the long life of the NKC-9 catalyst.

3.7. Characterizations of NKC-9. **3.7.1. Determination of the Pore Size Diameter Distribution of NKC-9.** The surface morphology of NKC-9 was clearly illustrated by its SEM image with a magnification of 50000× (Figure 11), which could get the idea of the pore size of the catalyst to a certain extent. The pore size diameter distribution curve of NKC-9 was determined

Table 5. Parameters and Results of Simulation and Optimization

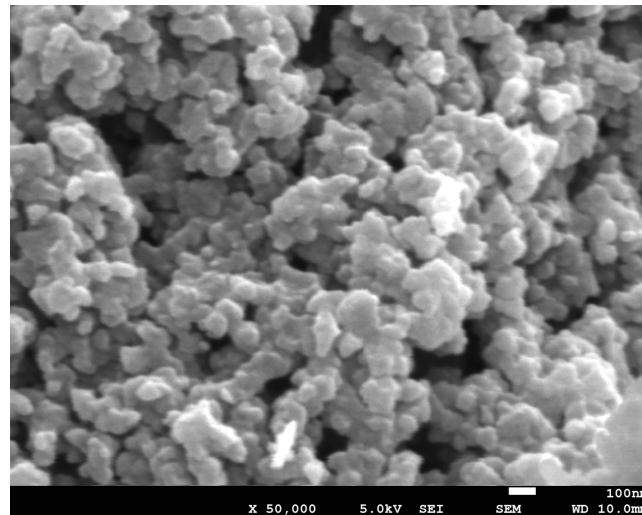
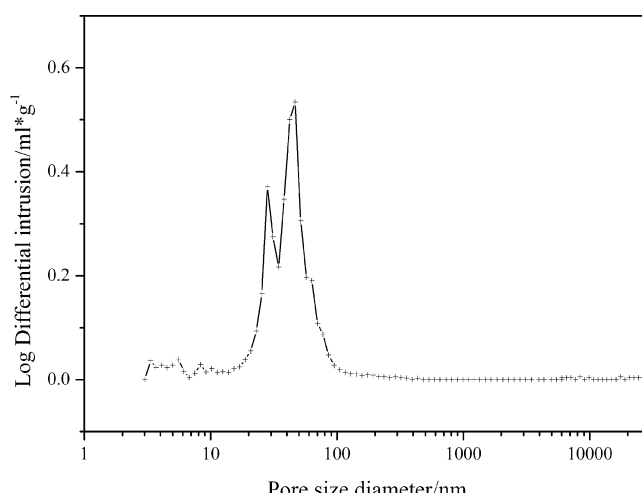
parameters	results
optimum stage number	45
optimum acid feeding position	10
optimum feeding position	40
optimum reflux ratio	1.3
feed θ_{Bo}	1.2
acetic acid conversion rate	$\geq 99.5\%$
methyl acetate concentrations in the tower top	$\geq 99.0\%$

**Figure 9.** Vapor–liquid composition distribution in catalytic distillation column.**Figure 10.** Lifetime evaluation of NKC-9.

by a mercury penetration method. As is shown in Figure 12, the pore size diameter was distributed from 30 to 80 nm, and the average pore diameter measured was 48.2 nm.

3.7.2. Determination of the S Content of NKC-9. NKC-9 resin mainly composed of C, H, O, and S. The content of C, H, and S was directly measured by the elemental analyzer, and the O content was obtained from the normalization method. The elements content of NKC-9 is shown in Table 6.

The hydrogen ion concentration reflects the total acidity of NKC-9. Because the sulfur (S) of NKC-9 exists in the form of $-\text{SO}_3\text{H}$, the hydrogen ion and sulfur ion have the same number

**Figure 11.** SEM image of NKC-9 with a magnification of 50000 \times .**Figure 12.** Pore size diameter distribution curve of NKC-9.**Table 6. Elements Content of NKC-9**

test	weight (mg)	C (%)	H (%)	S (%)	O (%)
1	2.055	39.410	5.918	12.766	41.906
2	1.982	39.690	6.026	12.769	41.515
3	2.005	39.710	6.006	12.712	41.572
4	2.039	41.330	6.042	13.271	39.357
5	1.985	40.820	5.966	13.064	40.150
6	2.034	41.110	6.018	13.139	39.733
average	40.345	5.996	12.954	40.706	

of moles. And the hydrogen ion concentration was calculated by the following equation:

$$\text{C}[\text{H}^+/\text{mol}\cdot(\text{g}\cdot\text{dry}\cdot\text{resin})^{-1}] = c(S) = \text{wt}\%(\text{S})/A_r(\text{S}) \quad (30)$$

where A_r is the relative atomic mass of S.

3.7.3. FT-IR. Figure 13 shows the FT-IR spectra of the fresh and regenerative NKC-9 catalyst. The broad band appearing in the range 3200 to 3400 cm^{-1} is due to OH stretching in the acidic cation exchange resins. The $-\text{OH}$ originated from $-\text{SO}_3\text{H}$ and water absorbed by the resins. The bands observed at approximately 1300 to 1510 cm^{-1} are attributed to C=C stretching (aromatic) vibrations. Two strong bands appeared at

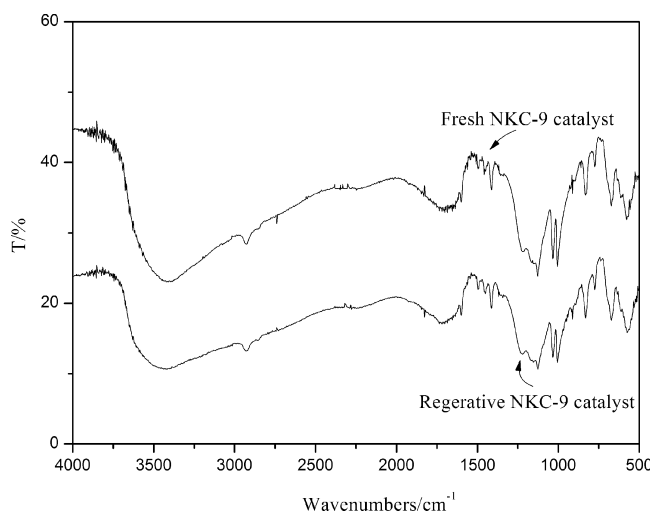


Figure 13. FT-IR spectra of the fresh and regenerative NKC-9 catalyst.

2940 to 2850 cm^{-1} due to the asymmetrical and symmetrical stretching vibrations of the $-\text{CH}_2$ group. The peak at 2350 cm^{-1} belongs to the absorption peak of carbon dioxide. The broad band appearing from 1670 to 1620 cm^{-1} is due to $\text{C}=\text{C}$ stretching in the ethenyl group. Several characteristic absorption peaks were observed from 500 to 1250 cm^{-1} , which verify the presence of $-\text{SO}_3\text{H}$. Moreover, the main peaks in the FT-IR spectra of the fresh catalyst are still present in the FT-IR spectra of the regenerative catalyst. The two FT-IR spectra were substantially identical, which demonstrated the good regeneration performance of strongly acidic styrene cation-exchange resin catalysts. The structural formula of the strongly acidic cation-exchange resin catalyst NKC-9 with $-\text{SO}_3\text{H}$ is illustrated in Figure 14.

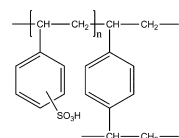


Figure 14. Structural formula of the strongly acidic cation-exchange resin.

3.7.4. XRD. The XRD patterns of the fresh and regenerative NKC-9 catalyst were obtained using a power X-ray diffractometer (Rigaku Dmax-C) with $\text{Cu K}\alpha$ radiation ($k = 1.5405 \text{ \AA}$). The XRD patterns were obtained from $2\theta = 10^\circ$ to 90° . As is clearly shown in Figure 15, three broad peaks are found at the 2θ range of 19.4° , 28.3° , and 42.1° for the fresh NKC-9. The other weak peaks can be attributed to monoclinic zirconia. The three main peaks at 19.4° , 28.3° , and 42.1° were still present in the XRD pattern of the regenerative NKC-9. In addition, the XRD pattern of the regenerative NKC-9 catalyst was almost identical with that of the fresh NKC-9 catalyst, which indicated the excellent regeneration performance of NKC-9 catalyst.

3.7.5. PM. Figure 16 shows the PM photomicrographs of the fresh and used NKC-9 catalyst in the fixed-bed reactor, the changes in the catalyst morphology are shown. Figure 16A is the surface morphology of the fresh catalyst. The fresh catalyst is an erratic ball with the smooth and uniform surface. Figure 16B,C,D shows the surface of the catalyst used in the fixed-bed reactor for over 1000 h with different amplification multiples.

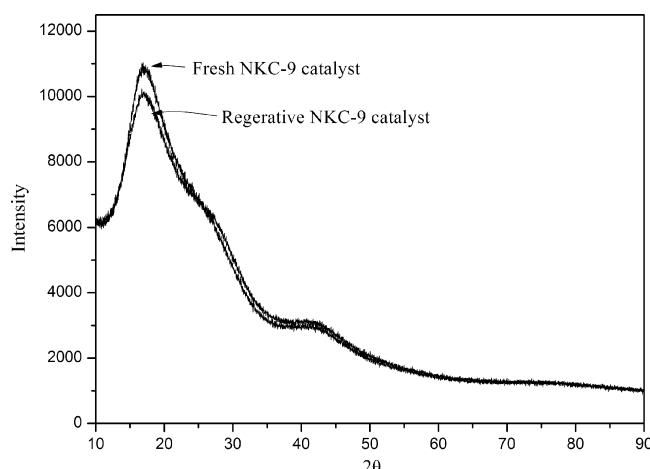


Figure 15. XRD patterns of the fresh and regenerative NKC-9 catalyst.

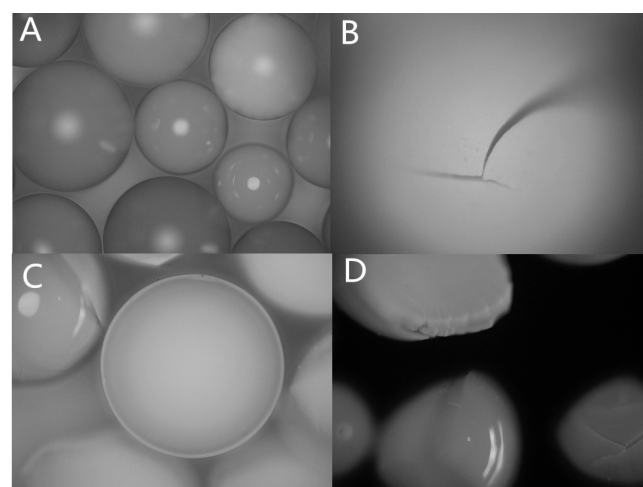


Figure 16. PM photomicrographs of the fresh and used NKC-9 catalyst in the fixed-bed reactor.

Cracks appeared on the catalyst surface (Figure 16B). The catalyst ball was fractured into the hemisphere (Figure 16C). A plastic deformation was found on the catalyst surface (Figure 16D).

The breakage rate of the catalyst in the fixed-bed reactor was approximately 5% as obtained from the calculations, but the breakage was largely attributed to the catalyst screening machine. In addition, the adsorption, deposition, and collision in the catalytic esterification process were also responsible for the deactivation of the catalyst. In summary, the NKC-9 catalyst is suitable for the methyl acetate synthesis in a catalytic distillation column.

4. CONCLUSIONS

NKC-9 has better catalytic activity than D072 for the esterification of acetic acid with methanol. Using NKC-9 as a catalyst, a catalyst load of 0.025 g catalyst/g liquid mixture, 60 °C, molar ratio of reactants of 1.2:1, stirring speed of 450 rpm, and catalyst particle size of >28 meshes were optimum operating parameters. K_{eq} and K_y of methyl acetate synthesis under different reaction temperatures were obtained, and the results of the kinetics data correlation indicated the LHHW model was capable of representing the kinetic behavior of the liquid–solid catalytic esterification. However, the results fitted

well when the P-H model was incorporated into the simulation. For methyl acetate synthesis, 1.5 h was the most appropriate space-time of the fixed-bed reactor. Good results were obtained from the simulation of catalytic distillation process. Long life and excellent regeneration performance of NKC-9 demonstrated it is suitable for methyl acetate synthesis in a catalytic distillation column.

■ ASSOCIATED CONTENT

Supporting Information

Physical properties of NKC-9 and D072. This material is available free of charge via the Internet at <http://pubs.acs.org>.

■ AUTHOR INFORMATION

Corresponding Authors

*Langsheng Pan. Tel/Fax: +86 73158298330. E-mail: panls97@126.com.

*Suojiang Zhang. Tel/Fax: +86 01082627080. E-mail: sjzhang@home.ipe.ac.cn.

Notes

The authors declare no competing financial interest.

■ ACKNOWLEDGMENTS

The authors gratefully acknowledge the National Natural Science Foundation of China (No. 51104140) and Petrochemical Joint Fund U1162106 and Beijing Nova Programme (Z12111000250000).

■ REFERENCES

- (1) Yu, W.; Hidajat, K.; Ray, A. K. Determination of adsorption and kinetic parameters for methyl acetate esterification and hydrolysis reaction catalyzed by Amberlyst 15. *Appl. Catal., A* **2004**, *260*, 191–205.
- (2) Gorak, A.; Hoffmann, A. Catalytic distillation in structured packings: Methyl acetate synthesis. *AICHE J.* **2001**, *47*, 1067–1076.
- (3) Fuchigami, Y. Hydrolysis of methyl acetate in distillation column packed with reactive packing of ion exchange resin. *J. Chem. Eng. Jpn.* **1990**, *23*, 354–359.
- (4) Lee, M. J.; Chiu, J. Y.; Lin, H. Kinetics of catalytic esterification of propionic acid and n-butanol over Amberlyst 35. *Ind. Eng. Chem. Res.* **2002**, *41*, 2882–2887.
- (5) Calvar, N.; González, B.; Dominguez, A. Esterification of acetic acid with ethanol: Reaction kinetics and operation in a packed bed reactive distillation column. *Chem. Eng. Process.* **2007**, *46*, 1317–1323.
- (6) Han, S. J.; Jin, Y.; Yu, Z. Q. Application of a fluidized reaction-distillation column for hydrolysis of methyl acetate. *Chem. Eng. J.* **1997**, *66*, 227–230.
- (7) Smejkal, Q.; Kolena, J.; Hanika, J. Ethyl acetate synthesis by coupling of fixed-bed reactor and reactive distillation column—Process integration aspects. *Chem. Eng. J.* **2009**, *154*, 236–240.
- (8) Sharma, M. M. Some novel aspects of cationic ion-exchange resins as catalysts. *React. Funct. Polym.* **1995**, *26*, 3–23.
- (9) Chakrabarti, A.; Sharma, M. M. Cationic ion exchange resins as catalyst. *React. Polym.* **1993**, *20*, 1–45.
- (10) Liu, W. T.; Tan, C. S. Liquid-phase esterification of propionic acid with n-butanol. *Ind. Eng. Chem. Res.* **2001**, *40*, 3281–3286.
- (11) Lee, M. J.; Wu, H. T.; Lin, H. Kinetics of catalytic esterification of acetic acid and amyl alcohol over Dowex. *Ind. Eng. Chem. Res.* **2000**, *39*, 4094–4099.
- (12) Xu, Y.; Dou, W.; Zhao, Y.; Huang, G.; Ma, X. Kinetics Study for Ion-Exchange-Resin Catalyzed Hydrolysis of Methyl Glycolate. *Ind. Eng. Chem. Res.* **2012**, *51*, 11653–11658.
- (13) Chang, Y. A.; Seader, J. D. Simulation of continuous reactive distillation by a homotopy-continuation method. *Comput. Chem. Eng.* **1988**, *12*, 1243–1255.
- (14) Song, W.; Venimadhavan, G.; Manning, J. M.; Malone, M. F.; Doherty, M. F. Measurement of residue curve maps and heterogeneous kinetics in methyl acetate synthesis. *Ind. Eng. Chem. Res.* **1998**, *37*, 1917–1928.
- (15) Huang, S. G.; Kuo, C. L.; Hung, S. B.; Chen, Y. W.; Yu, C. C. Temperature control of heterogeneous reactive distillation. *AICHE J.* **2004**, *50*, 2203–2216.
- (16) Sanz, M. T.; Murga, R.; Beltrán, S.; Cabezas, J. L.; Coca, J. Kinetic study for the reactive system of lactic acid esterification with methanol: Methyl lactate hydrolysis reaction. *Ind. Eng. Chem. Res.* **2004**, *43*, 2049–2053.
- (17) Xu, Z. P.; Chuang, K. T. Effect of internal diffusion on heterogeneous catalytic esterification of acetic acid. *Chem. Eng. Sci.* **1997**, *52*, 3011–3017.
- (18) Jiao, T.; Zhuang, X.; Li, C.; Zhang, S. A benzene chain-based contribution method for prediction of physical properties of aromatic compounds. *Fluid Phase Equilibr.* **2014**, *361*, 60–68.
- (19) Huang, Y.; Dong, H.; Zhang, X.; Li, C.; Zhang, S. A new fragment contribution-corresponding states method for physicochemical properties prediction of ionic liquids. *AICHE J.* **2013**, *59*, 1348–1359.
- (20) Li, C.; Zhang, X.; Zhang, S.; Suzuki, K. Environmentally conscious design of chemical processes and products: Multi-optimization method. *Chem. Eng. Res. Des.* **2009**, *87*, 233–243.
- (21) Li, C.; Wozny, G.; Suzuki, K. Design and synthesis of separation process based on a hybrid method. *Asia-Pac. J. Chem. Eng.* **2009**, *4*, 905–915.
- (22) Pöpken, T.; Steinigweg, S.; Gmehling, J. Synthesis and hydrolysis of methyl acetate by reactive distillation using structured catalytic packings: Experiments and simulation. *Ind. Eng. Chem. Res.* **2001**, *40*, 1566–1574.
- (23) Gmehling, J.; Onken, U. *Vapor-Liquid Equilibrium Data Collection-Aqueous Organic Systems*; DECHEMA Chemistry Data Series, Vol. 1, Part 1; DECHEMA: Frankfurt, 1977.
- (24) Gmehling, J.; Onken, U. *Vapor-Liquid Equilibrium Data Collection-Organic Hydroxy Compounds: Alcohols*; DECHEMA Chemistry Data Series, Vol. 1, Part 2a; DECHEMA: Frankfurt, 1977.
- (25) Gmehling, J.; Onken, U.; Grenzheuser, P. *Vapor-Liquid Equilibrium Data Collection-Carboxylic Acids, Anhydrides, Esters*; DECHEMA Chemistry Data Series, Vol. 1, Part 5; DECHEMA: Frankfurt, 1982.
- (26) Gmehling, J.; Onken, U.; Rarey-Nies, J. R. *Vapor-Liquid Equilibrium Data Collection-Organic Hydroxy Compounds: Alcohols (Supplement 3)*; DECHEMA Chemistry Data Series, Vol. 1, Part 2e; DECHEMA: Frankfurt, 1988.